Bringing physics to life at the submesoscale

Bringing physics to life at the submesoscale

Marina Lévy[1*], Raffaele Ferrari[2], Peter J.S. Franks[3], Adrian P. Martin[4], Pascal Rivière[5]

(1) LOCEAN-IPSL, CNRS/UPMC/IRD/MNHN, Paris, France

(2) Massachusetts Institute of Technology, Cambridge, USA

(3) Scripps Institution of Oceanography, UCSD, La Jolla, USA

(4) National Oceanography Centre, Southampton, SO14 3ZH, UK

(5) LEMAR-IUEM, CNRS/IRD/UBO, Plouzané, France

* Corresponding author, marina@locean-ipsl.upmc.fr

Draft, resubmitted version for GRL "Frontier Article", June 2012

Abstract

A common dynamical paradigm is that turbulence in the upper ocean is dominated by three classes of motion: mesoscale geostrophic eddies, internal waves and microscale three-dimensional turbulence. Close to the ocean surface, however, a fourth class of turbulent motion is important: submesoscale frontal dynamics. These have a horizontal scale of O(1-10) km, a vertical scale of O(100) m, and a time scale of O(1) day. Here we review the physical-chemical-biological dynamics of submesoscale features, and discuss strategies for sampling them. Submesoscale fronts arise dynamically through nonlinear instabilities of the mesoscale currents. They are ephemeral, lasting only a few days after they are formed. Strong submesoscale vertical velocities can drive episodic nutrient pulses to the euphotic zone, and subduct organic carbon into the ocean's interior. **The reduction of vertical mixing at submesoscale fronts can locally increase the mean time that photosynthetic organisms spend in the well-lit euphotic layer and promote primary production.** Horizontal stirring can create intense patchiness in planktonic species. Submesoscale dynamics therefore can change not only primary and export production, but also the structure and the functioning of the planktonic ecosystem. Because of their short time and space scales, sampling of submesoscale features requires new technologies and approaches. This paper presents a critical overview of current knowledge to focus attention and hopefully interest on the pressing scientific questions concerning these dynamics.

1- Introduction

The ocean's storage of carbon and ability to regulate atmospheric carbon dioxide is crucially dependent on primary production, the creation of organic matter from inorganic nutrients and carbon through photosynthesis. The transport of limiting nutrients to the sunlit surface ocean (the euphotic zone) plays a central role in controlling primary production. It has been argued that turbulent eddy motions are an important vehicle for this transport (Falkowski et al., 1991; Flierl and Davis, 1993; Oschlies and Garcon, 1998; Mahadevan and Archer, 2000; Martin and Richards, 2001; Levy et al., 2001; Williams and Follows, 2003). Although the subject of some debate (Oschlies, 2002; McGillicuddy et al., 2003; Martin and Pondaven, 2003) it has been claimed that in some regions of the ocean as much as half of the nitrate supply may be driven by eddy-induced vertical motions (McGillicuddy et al., 1998). The other essential ingredient for photosynthesis is light. Turbulent motions modulate the availability of light by moving phytoplankton through the euphotic zone (Sverdrup, 1953; Lévy et al., 1998; Taylor and Ferrari, 2011a). The nutrient and light environments that regulate global primary production, the export of fixed carbon to depth and ultimately the efficiency of the ocean's biological carbon storage, are thus intimately intertwined with these turbulent motions.

Until a few years ago, the dynamical paradigm was that turbulence in the upper ocean is dominated by three classes of motion: mesoscale geostrophic eddies, internal waves and microscale three-dimensional turbulence. Geostrophic eddies are generated through barotropic and baroclinic instabilities of the mean currents at mesoscales of O(10-100) km and dominate the eddy kinetic energy of the ocean. **The mesoscale eddies twist and fold tracer filaments resulting in a cascade of tracer variance to smaller scales, while they interact and pair resulting in a cascade of energy to larger scales. Internal waves, generated by surface winds and tidal forcing at scales O(0.1-10) km, interact and drive**

a transfer of energy toward smaller spatial scales. Microscale turbulence at scales O(0.01) km and less arises from three-dimensional instabilities driven by air-sea fluxes in the turbulent boundary layers and from breaking internal gravity waves in the interior. **The absence of an energy cascade to smaller scales separates mesoscale turbulence from internal waves and microscale turbulence that transfer energy to molecular dissipation scales.**

There is a rich literature on the impact of these three phenomena on biological dynamics in the ocean. Geostrophic eddies can regulate both the lateral (e.g., Williams and Follows, 1998; Oschlies, 2002; Lévy, 2003; Ferrari et al., 2008; Lehahn et al., 2011; Chelton et al., 2011) and vertical (e.g., McGillicuddy et al., 1998; Uz et al., 2001; Cipollini et al., 2001; Martin and Richards, 2001; McGillicuddy et al., 2007) transport of biomass and nutrients. Internal waves affect production by periodically heaving biomass into the euphotic zone (e.g., Holloway and Denman, 1989). Microscale turbulence maintains well-mixed biomass and nutrients within the turbulent surface boundary layer as well as driving nutrient fluxes into the mixed layer (e.g., Lewis et al. 1986) and particulate and dissolved organic carbon out of it (e.g., Ruiz et al., 2004).

Recent observations and numerical simulations, however, suggest that close to the ocean surface a fourth class of turbulent motion is important: submesoscale frontal dynamics (e.g. Thomas et al., 2008; Ferrari, 2011). Submesoscale fronts arise at scales just smaller than the mesoscale: a horizontal scale of O(1-10) km, i.e., less than the first baroclinic deformation radius; a vertical scale of O(100) m, i.e., thinner than the main thermocline; and a time scale of O(1) day. **Submesoscale fronts arise dynamically through advective interactions involving mesoscale currents (and thus are distinct from inertial-gravity waves on comparable spatial scales). They are, importantly, influenced by Earth's rotation and by density stratification (unlike microscale turbulence). Most importantly, submesoscale**

fronts are distinct from the filaments generated by mesoscale stirring, because they are characterized by density jumps and sharp velocity jets. Mesoscale stirring is inefficient at transferring potential (density filaments) and kinetic (narrow jets) energy to scales below the first deformation radius. Frontogenesis at the ocean surface (and other boundaries) breaks this constraint and results in a transfer of energy from the mesoscale to fronts and then all the way to dissipation through secondary frontal instabilities, as we discuss below. From the perspective of this review, the emergence of submesoscale fronts is particularly important because they can regulate the exchange of properties between the turbulent boundary layer and the ocean interior.

The relative contribution of the various turbulent motions to the evolution of a tracer is best illustrated in terms of the Reynolds-averaged equation – the equation describing the dynamics of the long-time average of the tracer. For illustrative purposes, let us consider the concentration of nutrient N averaged over a time/spatial scale larger than the mesoscale field. The average evolves according to:

$$\partial_t \overline{N} + \underbrace{\overline{u}.\nabla\overline{N}}_{mean} = -\underbrace{\nabla_H \cdot \overline{u'N'}}_{mesoscale} - \underbrace{\partial_z \overline{w'N'}}_{submesoscale} + \underbrace{\partial_z\left(\overline{k_z \partial_z N}\right)}_{microscale} + \underbrace{\overline{B(N)}}_{biology} \quad (1)$$

where overbars indicate averages and primes denote eddy fluctuations over this spatio-temporal scale. **For clarity, we have separated the microscale Reynolds fluxes, which are associated with irreversible mixing of water masses, and the mesoscale and submesoscale Reynolds fluxes, which represent advective transport of material properties along density surfaces without irreversible mixing.** The horizontal advective Reynolds fluxes are dominated by mesoscale eddies (Ledwell et al., 1998). The vertical advective Reynolds fluxes are dominated by mesoscale eddies in the ocean interior away from boundaries, but there is growing evidence that in the upper few hundred meters of the

oceans they are dominated by submesoscale circulations at fronts **(e.g., Capet et al., 2008; Klein and Lapeyre, 2009); evidence of the more active role of submesoscales in the vertical Reynolds flux is presented in section 3.3.** The effect of microscale turbulence often referred to as vertical mixing, is particularly strong in the turbulent boundary layers, where it keeps tracers and momentum well mixed. In this equation it is parameterized as a vertical diffusivity term, with k_z the vertical diffusion coefficient. Finally, *B(N)* denotes all biological processes affecting the concentration of *N*. Typically, for nitrate *B(N)* includes uptake by phytoplankton and production through nitrification. An equation similar to Eq. (1) holds for phytoplankton, except that the "biology" term accounts for phytoplankton growth minus losses such as death and respiration.

The potential role of the submesoscale has only recently been recognized; thus, compared to the other terms in the above equation little is known about its magnitude, distribution and contribution to vertical and horizontal fluxes. This paper presents a critical overview of current knowledge to focus attention and hopefully interest on the pressing scientific questions concerning these dynamics.

The paper is organized into 6 parts. Section 2 reviews the main characteristics of submesoscale dynamics. Section 3 examines how these dynamics are likely to affect the nutrient and phytoplankton budget of the euphotic layer. Section 4 focuses on the impact of submesoscale dynamics on the structure and spatial distributions of the planktonic ecosystem. Section 5 discusses the observational difficulties associated with investigating submesoscale heterogeneities. Finally, section 6 comprises the Conclusions.

2- Submesoscale dynamics

Stirring by large-scale ocean currents and mesoscale eddies creates a convoluted web of filaments of all oceanic tracers, including temperature, salinity, nutrients and phytoplankton. However, only close to the ocean surface does the filamentation of hydrographic properties evolve into sharp density fronts with associated strong submesoscale circulations (Fig.1). **The theory of frontogenesis at the ocean surface is well understood and the interested reader is referred to the many excellent in-depth reviews (e.g., Hoskins, 1982; Thomas et al., 2008; Klein and Lapeyre, 2009). Here we offer a heuristic argument to explain why submesoscale fronts are generated preferentially at the ocean surface. Note that fronts can also be generated at the ocean bottom, but our focus is on the impact of fronts on ocean productivity in the upper ocean.**

At the mesoscale, i.e., scales larger than the first deformation radius of O(10-100) km (Chelton et al., 1998), the pressure gradients associated with horizontal density fronts are balanced by the Coriolis acceleration due to Earth's rotation: the so-called "geostrophic balance". The degree of geostrophic balance is quantified in terms of the Rossby number $Ro=U/fL$, where U is the characteristic velocity at a front, L is the frontal width and f is the Coriolis parameter: geostrophic balance holds if $Ro<<1$. **In the ocean interior, density surfaces are very flat with a steepness smaller than *O(Ro)*. Whenever the mesoscale or large-scale velocity field is locally convergent and acts to compress and steepen density surfaces, an overturning circulation develops that promptly brings the surfaces back toward the horizontal (reducing their steepness) and restores the geostrophic balance (increasing *L*). Hence submesoscale motions with *Ro*=O(1) do not arise spontaneously in the ocean's interior. A convergent velocity field, however, compresses passive tracers that have no feedback on the dynamics. Indeed mesoscale turbulence in the ocean interior continuously generates sharp tracer filaments, a process referred to as a**

158 **forward cascade of enstrophy and tracer variance (Charney, 1971). It is only density**
159 **surfaces that remain smooth (Lapeyre et al., 2006; Klein et al., 2008).**

160 **The situation is quite different at the ocean surface. In regions of flow convergence**
161 **where density surfaces are brought together, the overturning circulation, that in the**
162 **interior slumps surfaces back to the horizontal, becomes purely horizontal at the**
163 **surface because water cannot cross the air-sea interface. The horizontal circulation acts**
164 **to further accelerate the convergence of density surfaces resulting in frontogenesis – the**
165 **formation of sharp density fronts in a time of a few days (Hoskins and Bretherton,**
166 **1972; Spall, 1995). As the fronts form, the slope of the density surfaces increases (the**
167 **slope is further increased by microstructure turbulence in the surface mixed layer**
168 **which mixes away any vertical stratification) and *Ro* becomes O(1). The increase in *Ro***
169 **results in strong ageostrophic submesoscale circulations that drive a forward energy**
170 **cascade and excite local microstructure turbulence (Molemaker and McWilliams, 2010;**
171 **Taylor and Ferrari, 2010). The increase in slope is accompanied by the development of**
172 **intense upwelling and downwelling on the warm and cold sides of the front respectively:**
173 **the ratio of vertical to horizontal velocities scales with the slope of density surfaces and**
174 **it is therefore much larger at fronts.** In the ocean interior, with frontal aspect ratios of
175 $O(10^{-4} - 10^{-3})$ and horizontal velocities of O(0.1) m/s, the vertical velocities reach $O(10^{-5}\text{-}10^{-4})$
176 m s^{-1} or O(1-10) m d^{-1}. Near the surface the vertical velocities reach $O(10^{-3})$ m s^{-1} or O(100)
177 m d^{-1} (Mahadevan and Tandon, 2006; Legal et al., 2007; Klein and Lapeyre, 2009). These
178 large vertical velocities extend from just below the surface down to a few hundred meters and
179 drive a rapid exchange of properties between the turbulent boundary layer and the permanent
180 thermocline (Fig.2a).

181 Submesoscale fronts are ephemeral and typically last only a few days after they are
182 formed. This is either because the flow convergence ceases as currents and mesoscale eddies

183 evolve, or because the fronts become unstable. During frontolysis (frontal decay) the vertical
184 velocity and the associated exchange of properties with the ocean interior progressively
185 decrease. The shutdown is particularly rapid and extreme when frontolysis is associated with
186 frontal instabilities (Boccaletti et al., 2007; Capet et al., 2008; Thomas and Ferrari, 2008),
187 sometimes taking just a few hours. There is a rapidly growing literature on the details of how
188 such instabilities develop. In the first stage, light waters flow over dense waters in what is
189 called symmetric instability, a process that has recently been observed at the Kuroshio
190 (D'Asaro et al., 2011) and Gulf Stream fronts (Thomas and Joyce, 2010). Later, meanders
191 and eddies develop along the front and slumping accelerates as a result of baroclinic
192 instability (Fox-Kemper et al, 2008). Other forms of instability have also been reported when
193 the lateral shear at the front is particularly intense (McWilliams, 2010). Regardless of the
194 details of specific processes, the instabilities typically result in restratification and
195 suppression of vertical mixing within the turbulent boundary layer **(i.e. a strong decrease of**
196 $\boldsymbol{k_z}$ **in Eq. 1).**

197 Thomas (2005) points out that frontolysis can be arrested by winds. If the winds blow in
198 the same direction as the frontal current, they act to steepen the front and prevent further
199 slumping by frontal instabilities. In such situations turbulent mixing is enhanced at fronts,
200 rather than being reduced, and no restratification takes place (e.g., Franks and Walstad,
201 1997). If the winds blow in the opposite direction of the frontal current they act to slump the
202 front, further accelerating restratification by frontal instabilities.

203 In summary, one expects frontogenesis whenever large-scale currents or mesoscale eddies
204 converge to bring together different water masses. During this phase strong vertical velocities
205 develop which promote exchange of properties between the surface ocean and the permanent
206 thermocline. Once the convergent flow weakens, frontolysis effectively suppresses turbulent
207 mixing at the front except when winds blow in the direction of the frontal current.

3- Response of phytoplankton to submesoscale dynamics

The response of phytoplankton to submesoscale dynamics will typically depend on what factor exerts the main control over phytoplankton growth, light or nutrients. In case of nutrient limitation, the contribution of the submesoscale is mostly through the supply of nutrients into the nutrient starved euphotic layer. However, some of the most productive regions are in the high latitudes, where spring blooms are light limited. In the case of light limitation, the impact of submesoscales is mostly to modulate the strength of vertical mixing and thus the light exposure of phytoplankton. Moreover, in both cases, submesoscale processes will export phytoplankton out of the surface layer. These mechanisms, how they combine and their potential impact on large scale fluxes, are presented in this section.

3.1 Response to submesoscale vertical transport

Over much of the ocean, phytoplankton growth is constrained by the availability of nutrients, which are abundant beneath the euphotic zone. The upward component of the submesoscale vertical circulation enhances the nutrient flux into the euphotic layer, stimulating phytoplankton growth (Fig. 2a) (Mahadevan and Archer, 2000; Levy et al., 2001; Allen et al., 2005; Lapeyre and Klein, 2006b; Nagai et al., 2008; Johnson et al., 2010; Pidcock et al., 2010). Submesoscale upwelling can also drive deep phytoplankton biomass upward, alleviating light limitation of growth (Lévy et al., 2001). The downward branch, however, has a negative impact on primary production by subducting phytoplankton, together with other organic matter, out of the euphotic zone (Fig. 2a) (Kadko et al., 1991; Fielding et al., 2001; Levy et al., 2001; Niewiadomska et al., 2008; Thomas and Joyce, 2010). This subduction acts as a physical carbon pump and modifies the properties of intermediate mode waters (Karleskind et al., 2011a,b). Submesoscale vertical motions will occur in all regions,

not just those that are nutrient limited. Purely from a perspective of vertical transport, therefore, the net biogeochemical effect of submesoscale dynamics may vary with region, representing a changing balance of the two antagonistic effects (Lathuilière et al., 2010). The strength of the submesoscale vertical advection also varies in space and time depending in part on the intensity of the eddy activity, and can be enhanced by winds through the generation of inertial motions (Franks and Walstad, 1997) that interact with the submesoscale frontogenetic dynamics (Lévy et al., 2009).

Much of our knowledge on this topic comes from models. For example, simulations suggest that submesoscale turbulence increases phytoplankton abundance in the open ocean (Lévy et al., 2001, Oschlies, 2002, McGillicuddy et al., 2003) but decreases it in eastern boundary upwelling regions (Lathuilière et al., 2011). Some studies also suggest that in regions where nutrients are plentiful, such as the subpolar North Atlantic or eastern boundary upwelling systems, submesoscale vertical circulations could cause a loss of nutrients from the euphotic layer (Lévy et al., 2000; Oschlies, 2002, McGillicuddy et al., 2003, Gruber et al., 2011). More generally, the regional net flux of nutrients due to submesoscale vertical advection depends on the often strongly localized distribution of enhanced vertical circulation and the rate of removal of upwelled nutrients from the upwelling regions by horizontal advection (Martin et al., 2002; Martin et al., 2003; Pasquero et al., 2005). Typically, capturing the full strength of submesoscale vertical movements requires horizontal model resolution of the order of one tenth of the internal Rossby radius of deformation. This would require a resolution of O(1) km at mid-latitudes, though this depends on the mixed-layer depth. Studies with a coarser resolution will not fully capture the vertical circulation.

There are only a few observational studies to complement these model results: the balance between upwelling and subduction of nutrients, phytoplankton and other organic material is inherently difficult to assess purely from observations, let alone quantifying how

this balance varies with the intensity of submesoscale turbulence. The magnitude of submesoscale turbulence can be evaluated from mean properties such as eddy kinetic energy or descriptors such as the Lyapunov exponent of the flow. This approach to quantifying the link between the vertical transport of nutrients and the strength of the submesoscale flow was applied by Rossi et al. (2008) and Gruber et al. (2011) in eastern boundary upwelling regions and by Calil and Richards (2010) in the oligotrophic open ocean. These studies report a positive correlation between productivity and eddy kinetic energy derived from altimetry in the open ocean, but the opposite relationship for eastern boundary upwelling regions. Although it is too early to discern any clear pattern, these results are at least consistent with the modelling studies described earlier.

Submesoscale upwelling of nutrients to the surface also depends on how deep the submesoscale vertical velocities extend into the water column. The strength of the submesoscale vertical circulation is typically maximal at the base of the mixed layer. In situations of nutrient limitation, the largest vertical gradient of dissolved nutrients, the nutricline, is found at the base of the euphotic layer. The mixed layer is often shallower than the nutricline. In this case submesoscale upwelling will not be effective in mixing nutrients into the euphotic zone. A few studies have suggested that significant submesoscale vertical velocities can, in some circumstances, penetrate deeper than the mixed layer, potentially reaching the nutricline (Capet et al., 2008; Lévy et al., 2010). In contrast to the submesoscale, the mesoscale vertical circulation is maximal at the zero crossing of the first baroclinic mode, which is often found deeper in the water column (~500-1000 m).

The time scales associated with upwelling will also determine its influence on primary production: the delivery of nutrients by mesoscale eddies may be more efficient than submesoscale motions for biological growth (McGillicuddy et al., 2007). Though the vertical velocities associated with mesoscale eddies are much smaller than the submesoscale ones due

to the different *Ro* of the two regimes, the residence time of nutrients in the euphotic layer is longer for mesoscale eddies than for submesoscale fronts, potentially allowing for more complete uptake of the upwelled nutrients. Submesoscale fronts bring nutrients so rapidly in and out of the euphotic layer that it is unclear whether phytoplankton can fully utilize them. **Indeed, typically, the time scale of nutrient supply at the surface by submesoscale vertical velocities is of the order of 0(1-10) day, which corresponds to the time scale of nutrient uptake by phytoplankton.** Our current — rather incomplete — view of how the relationship between submesoscale and mesoscale vertical velocities varies with depth and time is a topic that clearly requires further research.

Finally, in terms of carbon, how the air-sea CO_2 exchange is affected by submesoscale vertical transport is not straightforward. For instance, there are compensating effects of the small-scale upwelling of nutrients and cold temperatures, which tend to decrease oceanic pCO_2, and the upwelling of dissolved inorganic carbon (DIC), which tends to increase it (Mahadevan et al., 2004; Mahadevan et al., 2011). The leading term of this balance depends on the relative vertical gradients of DIC (and alkalinity), nitrate and temperature. In the Northeast Atlantic, large submesoscale surface pCO_2 gradients have been observed, but attributed to stirring by mesoscale eddies rather than to vertical advection associated with submesoscale circulations (Resplandy et al., 2009).

3.2 Response to reduced vertical mixing at submesoscale fronts

When light is the main factor limiting phytoplankton production, such as in large parts of the Southern Ocean or at high latitudes prior to the spring bloom, the reduction of vertical mixing induced by submesoscale dynamics can locally increase the mean time that photosynthetic organisms spend in the well-lit euphotic layer and promote primary production. **This can be rationalized by the reduction of k_z in Eq. 1, with the consequence**

306 **of limiting phytoplankton excursions out of the euphotic layer (Fig. 2b).** Models suggest
307 that this reduction of vertical mixing can either result in a reduction in the mixed-layer depth
308 (Lévy et al., 1998) or in a reduction of mixing intensity within the mixed-layer (Taylor and
309 Ferrari, 2011a,b). This may lead to the beginning of a bloom prior to seasonal stratification,
310 and has been reported in the North Atlantic by Townsend et al. (1994) and Joyce et al.
311 (2009), as well as in the Adriatic by Santoleri et al. (2003). Model studies of this
312 phenomenon in the Mediterranean Sea (Lévy et al., 1999, 2000) suggest that it only modifies
313 the annual mean budget of phytoplankton production in the absence of strong seasonality.
314 Otherwise, the main effect seems to be restricted to the earlier onset of the bloom (Lévy et al.,
315 2005; Taylor and Ferrari, 2011a,b**). The importance of this process over large-scale, light-**
316 **limited regions (such as in the Southern Ocean) remains to be assessed.**

317 **3.3 Response to large-scale changes of the circulation induced by submesoscale**
318 **dynamics**

319 The effects on nutrients of local mesoscale and submesoscale perturbations of the
320 velocities do not cancel out when averaged over a regional scale. This is due to the non-linear
321 nature of advection. Mathematically, this local effect is associated with the Reynolds terms
322 (see Eq. 1). However, a complete picture of the impact of submesoscale turbulence on
323 nutrients has to account not only for the local Reynolds fluxes but also for how the
324 distribution of the large-scale circulation and nutrient fields (and hence the mean advection
325 and vertical diffusion) are modified by submesoscale phenomena. For instance, the feedback
326 of the submesoscale motions on the mean circulation may influence the position and strength
327 of western boundary currents, and through the thermal wind balance, the global equilibration
328 of the thermocline and nutricline (Lévy et al., 2010). In this sense there is an effect that is
329 non-local in space and time, and can be thought of as the remote effect of the submesoscale
330 dynamics. To demonstrate this impact it is necessary to run model experiments long enough

to allow the model mean state to equilibrate in the presence of submesoscale dynamics. Clearly there is a practical issue of the computational demands associated with this. One example, however, is provided by the model study of Levy et al. (2012). Here, phytoplankton abundance at equilibrium was found to be less in the submesoscale-resolving (1/54°) model than in the model without submesoscale processes. This result arises from the different large-scale distributions of the nutricline depth and mixed-layer depth in the two model equilibria.

An attempt to quantify the contribution of submesoscales to the annual nitrate balance in the euphotic layer at mid-latitudes is presented here in the context of the Lévy et al. (2012) model. A seasonally varying double-gyre is simulated, representative of an idealized sector of the Northwest Atlantic or Pacific. A strong surface jet, the model's equivalent of the Gulf Stream or Kuroshio, flows eastward at ~30°N (Fig. 3a). The instability of this jet generates intense mesoscale turbulence which is maximum in the vicinity of the jet but can be found throughout the region 20-40°N**. The submesoscale circulation can be seen in the form of submesoscale jets (Fig. 3a), accompanied by intense upwellings and downwellings on either sides of the jets (Fig. 3b). The nutrient concentration at the surface is characterized by a large-scale gradient, characteristic of the North Atlantic, and distorted by mesoscale stirring (Fig. 3c).** The long model spin-up (50 years) allows the annual mean position of the jet, as well as the thermocline and nutricline depths to reach equilibrium, integrating the feedback of submesoscale processes on large-scale quantities.

The model domain is large enough to encompass different biological regimes: an oligotrophic regime in the subtropical gyre (from ~20-30°N) where winter nitrate concentrations are less (Fig. 3c), a strong spring bloom in the subpolar gyre north of ~40°N and a mid-latitude regime with a moderate bloom between 30-40°N in the inter-gyre region. This north-south gradient in productivity is reflected by the structure of the biological term *B(N)* (Fig. 4).

At equilibrium, an annual integration of all the terms in equation (1) implies that $\partial_t N$ is zero and thus the biological term $B(N)$ is exactly balanced by the sum of the four physical terms. After integration over the euphotic depth, this leads to:

$$\int_{1year}\int_{z=0}^{Zeupho}[\underbrace{-\overline{u}.\nabla\overline{N}}_{remote}-\underbrace{\nabla_H\cdot\overline{u'N'}}_{mesoscale(local)}-\underbrace{\partial_z\overline{w'N'}}_{submesoscale(local)}+\underbrace{\partial_z\left(\overline{k_z\partial_z N}\right)}_{remote}]dzdt=\int_{1year}\int_{z=0}^{Zeupho}\underbrace{\overline{B(N)}}_{bio\log y}dzdt \quad (2)$$

The remote effect of submesoscales enters this equation through the mean advection and the vertical mixing terms. This is because submesoscale dynamics influence the mean currents, the mixed-layer depth and the mean distribution of nutrients. **The local effects enter the equation through the horizontal and vertical Reynolds fluxes. Here, the separation between mean and eddy fields was done with a space filter with a cut-off scale of O(100) km. Thus the Reynolds terms potentially contain the contribution of both the mesoscale and the submesoscale. However, spectra of horizontal and vertical nitrate flux vs. wavenumber k show that the horizontal flux spectrum (slope of $\sim k^{-2}$) is steeper than the vertical flux spectrum (slope of $\sim k^{-1}$) and implies that the integral over wavenumbers is dominated by the largest scales (small wavenumbers) in the case of the horizontal flux, but it is strongly affected by the smallest scales (large wave numbers) in the case of the vertical flux. The overall vertical tracer flux is thus strongly affected by the submesoscale fronts.**

The contribution of the different terms in Eq. 2 to the annual balance of nutrient supply to the euphotic layer varies regionally (Fig. 4), as does the relative importance of the local (Reynolds) and remote (mean) submesoscale contributions. Vertical mixing dominates the balance in the regions where the mixed layer gets deeper than the euphotic depth over the seasonal cycle. This is the case north of 40°N and in the eastern sector. In these regions the local submesoscale term is negligible. In contrast, in the intergyre region (30-40°N), the

379 mean and mesoscale advection terms are larger than vertical mixing and tend to oppose each
380 other. In this region the local submesoscale term has a magnitude comparable to the other
381 advective terms and is always positive. Thus, in this region local submesoscale advection is
382 efficiently supplying nitrate to the euphotic layer; this supply makes a substantial contribution
383 to the overall balance.

384 **4- Ecosystem response to submesoscale dynamics**

385 All the submesoscale dynamics described previously have the potential to change not
386 only the primary and export production, but also the structure and the functioning of the
387 planktonic ecosystem. Strong submesoscale vertical velocities can drive episodic nutrient
388 pulses into the euphotic zone, while horizontal stirring can create intense patchiness in
389 planktonic species. These processes have been investigated with both models and data.

390 Many field studies have observed systematic changes in phytoplankton community
391 structure across trophic gradients: the fraction of total biomass contributed by the smallest
392 cells decreases strongly with increasing biomass (e.g., Yentsch and Phinney, 1989; Chisholm,
393 1992; Ciotti et al., 2002; Li, 2002; Irigoien et al., 2004; Uitz et al., 2006). Biomass is
394 typically added in successively larger size classes as the total biomass increases, while
395 smaller size classes remain relatively unchanged (Landry, 2002).

396 These large-scale patterns are also seen in ecosystem responses to the episodic addition of
397 limiting nutrients. Cavender-Bares et al. (2001) measured size-abundance spectra of
398 phytoplankton in mesocosms of Sargasso Sea water enriched with NO_3 and PO_4 and found
399 that waves of enhanced biomass propagated from small to large sizes over 5 days. Similar
400 analyses inside iron-fertilized patches during IronEx II showed peaks and troughs of particle
401 abundance propagating toward the larger sizes of the size spectrum over 8 days with large
402 pennate diatoms dominating the increase in phytoplankton biomass (e.g., Coale et al., 1996;

403 Landry et al., 2000). This ecosystem response to enrichment is an emergent property driven
404 by the size-dependencies of fundamental biological rates such as growth, production and
405 grazing (e.g., Rassoulzadegan and Sheldon, 1986; Fuchs and Franks, 2010; Poulin and
406 Franks, 2010). Pulses of biomass propagating to larger size classes after a nutrient injection
407 reflect changing balances of growth and predation with size and time. These imbalances can
408 lead to disproportionate growth of larger phytoplankton and efficient food chains fueling
409 pelagic fish production (e.g., Moloney and Field, 1991). They can also lead to episodic
410 particle fluxes and locally enhanced carbon sequestration (e.g., Guidi et al., 2007). It is thus
411 critical to measure and understand the size-dependencies of phytoplankton growth and
412 microzooplankton grazing rates in submesoscale features where such pulses may be focused.

413 The changes in the size structure of the planktonic community driven by nutrient pulses
414 will lead to local patches of distinct species abundances. Such patches will become stirred
415 and distorted by the mesoscale and submesoscale horizontal velocity fields (Martin et al.,
416 2001). By combining multisatellite data, notably high-resolution ocean-colour maps of
417 dominant phytoplankton types and altimetry-derived Lagrangian diagnostics of the surface
418 transport, d'Ovidio et al. (2010) demonstrated that the phytoplankton landscape is organized
419 into submesoscale patches, often dominated by a particular phytoplankton group, separated
420 by physical fronts induced by horizontal stirring. These physical fronts effectively delimit
421 ephemeral ecological niches by encircling water masses of similar history and whose
422 lifetimes are comparable to the timescale of the biological response (a few weeks). This
423 submesoscale structuring of the plankton community is a direct consequence of horizontal
424 stirring by the turbulent circulation.

425

426

427 **4.1 Size-dependent ecosystem response to a nutrient pulse**

428 To explore the size-dependent community response to a nutrient pulse, we used the
429 Poulin and Franks (2010) (hereafter PF10) size-structured ecosystem model, which allows for
430 an arbitrary number of different size classes of phytoplankton *P* and zooplankton *Z* (typically
431 >500 size classes of each). The model is similar to the Fuchs and Franks (2010) size-
432 structured model: it is based on a simple NPZ model structure, but includes potential size-
433 dependence of all biological processes (growth, grazing, assimilation efficiency, etc.). The
434 results shown here were obtained with a herbivore-only model.

435 The PF10 model was initialized at steady state with a total nutrient concentration
436 (phytoplankton+zooplankton+dissolved nutrients) of 10 mmolN m^{-3} and given a nutrient
437 pulse of 5 mmolN m^{-3} over 1 day (Fig. 5). There was an immediate growth response across
438 all phytoplankton size classes. Over the days following the initial response, the smallest
439 phytoplankton showed the largest increase in biomass, followed by an increase in the biomass
440 of their grazers**. The increase of the grazers led to eventual net decreases in the smallest**
441 **phytoplankton. This grazer-induced decrease in the smallest phytoplankton decreased**
442 **their competitive ability, allowing growth of the larger phytoplankton.** Over the next 10
443 days (and longer), a pulse of high biomass propagated from the smallest phytoplankton
444 toward the largest. The duration of the biomass pulse depends on the phytoplankton growth
445 and zooplankton grazing rates; the pulse propagates more slowly and is of longer duration as
446 it reaches the larger (slower-growing) phytoplankton. **The phytoplanktonic biomass pulse**
447 **in a given size class is ultimately terminated by a subsequent biomass increase of the**
448 **herbivores. These results suggest that in a Lagrangian sense, nutrient pulses to the**
449 **euphotic zone should lead to a patchy, distinct, and evolving planktonic community**
450 **structure compared to surrounding waters. The resonance between the time scales of**
451 **submesoscale-driven nutrient injections (O(1) day, e.g., D'Asaro et al., 2011) and**

phytoplankton and protist grazer growth rates (O(1) d^{-1}) are expected to lead to significant modification of the planktonic community and its dynamics in the vicinity of submesoscale features.

4.2 Spatial diversity driven by submesoscale nutrient pump

The PF10 model is presently too computer intensive to run at full resolution in a 3D submesoscale-resolving model. To investigate the effects of submesoscale dynamics on spatial patterns of phytoplankton diversity, a reduced NPPZD (nutrient-phytoplankton-phytoplankton-zooplankton-detritus) model was run with a SQG (surface quasi-geostrophic) physical model (Perruche et al., 2011). In this model the phytoplankton community comprises two size classes of phytoplankton (P_1 and P_2), representing nano and micro phytoplankton respectively, using the Moloney and Field (1991) parameterization of growth rates. In particular, because of competitive exclusion there is no region of the parameter space (total nutrient C_o vs. irradiance I) in which P_1 and P_2 can coexist at equilibrium (Fig. 6c).

When coupled to the SQG model, the local perturbations of nutrients by physical processes nevertheless allow the coexistence of the two phytoplankton types (Fig. 6ab): P_2 dominates in the long thin filaments between eddies formed by the straining of the concentration fields; P_1 dominates inside eddies, but is also found in the filaments. Both the coexistence and shifts in the balance of this coexistence over short length scales can be explained by considering the response time scales of the system (Fig. 6c). The similarity between the short time scales associated with strong submesoscale vertical nutrient injections and the ecosystem response time scale (given along the red line, Fig. 6c) favours dominance by the largest phytoplankton size class. On the other hand, the longer time scales associated with eddies with low rates of vertical nutrient injection favor the smallest phytoplankton class. The potential resonances between different components of the plankton and different

476 scales of physical forcing lead to strong spatial and temporal heterogeneities in community
477 structure and dynamics.

478 These nascent modelling studies underscore the importance of resolving submesoscale
479 features in models and in sampling. Biological processes such as growth, grazing,
480 aggregation and predation are all expected to be enhanced in submesoscale upwellings.
481 Nutrient pulses are able to propagate through the trophic web, driving strong changes in
482 community structure. The spatial and temporal heterogeneity of nutrient pulses, combined
483 with horizontal stirring, alters the competitive balance among different phytoplankton
484 species. We thus expect to see strong spatial and temporal gradients in planktonic community
485 structure forced by submesoscale physical dynamics. Furthermore, Cotté et al. (2011) and
486 Tew-Kai et al. (2009) have recently shown that the effects of submesoscale dynamics extend
487 through the food web to affect the top predators' foraging behaviour. Thus, the combined
488 effects of submesoscale features, even though a relatively small fraction of the total area, may
489 be disproportionately important to biological dynamics.

490 **5- Observational considerations**

491 A major obstacle to testing current predictions from theories and models is the difficulty
492 of adequately sampling the submesoscale. As mentioned above, the phenomena of interest are
493 both ephemeral and localized, taking just a few days to wax and wane and only being of O(1-
494 10) km in width despite being up to hundreds of kilometers in length. A major aspect of the
495 observational challenge, therefore, is one common to the purely physical study of the
496 submesoscale: the need to be able to survey a region at sufficiently high temporal and spatial
497 resolution.

498 Gliders (e.g., SPRAY spray.ucsd.edu/pub/rel/index.php, Slocum
499 www.webbresearch.com/slocumglider.aspx, Seaglider

500 www.irobot.com/gi/maritime/1KA_Seaglider) are fast becoming the platform of choice in a
501 wide range of oceanographic applications. Typically a glider can cover 1 km horizontally in
502 an hour with an ascent angle of around one in five. Steeper angles of ascent are possible but
503 with the consequence of slower horizontal progress. Even for larger submesoscale features of
504 O(10) km width a glider would require half a day for one transect. The slow speed also means
505 that the strong directional currents associated with many of the submesoscale features of
506 interest have the potential to displace the glider significantly over even one transect.

507 A more traditional alternative is a ship-towed undulating device, such as the SeaSoar
508 (Pidcock, 2011) or Triaxus (D'Asaro et al., 2011) platforms. These allow sampling typically
509 10-20 times faster than a glider, permitting much better time resolution of the evolution of
510 submesoscale features. Furthermore, the physical connection to the ship allows the use of
511 sensors whose power demands would significantly curtail the range of a glider. The costs of
512 and demands on research vessels mean that such studies are nevertheless limited in duration
513 relative to gliders, which can continue to sample a region for months even during the winter
514 period.

515 The relevant submesoscale timescales for a study impose other constraints on a study of
516 their biogeochemistry. An obvious intention might be to record biogeochemical processes
517 such as primary production and export of carbon over an annual cycle at a resolution
518 sufficient to allow the contribution of the submesoscale to be assessed. Given the fleeting
519 existence of any specific submesoscale feature this annual budget may best be addressed
520 using Eulerian sampling, building up a statistical picture of the cumulative effect of
521 submesoscale processes at a fixed location. The problem then arises of how temporal signals
522 in biogeochemistry can be disentangled from simple advection of spatial variability through
523 the site. Having a collection of moorings spaced at distances sufficient to resolve
524 submesoscale spatial variability might be one approach. The spatial coverage would also be

525 required to separate out the regional change in time associated with biological processes such
526 as nutrient uptake, population growth and sedimentation. This approach to studying the
527 underlying physical processes of the submesoscale is to be tried, for example, by the UK
528 OSMOSIS program, with the moorings augmented by gliders.

529 If study of the dynamics associated with a specific submesoscale feature is of interest then
530 a Lagrangian approach is required, as the mesoscale circulation may advect any feature tens
531 of kilometers in just one day. For example, D'Asaro et al. (2011) used a neutrally buoyant
532 float to mark a submesoscale front in the Japan Sea. They used this as a moving reference
533 point for repeated Triaxus surveys of the physical characteristics. A similar observational
534 strategy, augmented with fluorescence and backscattering measurements, was followed
535 during the 2008 North Atlantic spring bloom experiment (Fennel et al., 2011; Alkire et al.,
536 2012; D'Asaro, pers. comm.). A major program of the US Office of Naval Research targeting
537 the physics of the submesoscale will also use a Lagrangian approach. Two recent
538 developments that show considerable potential for Lagrangian studies involve the use of
539 multiple drifters. The Autonomous Underwater Explorer (http://jaffeweb.ucsd.edu/node/81)
540 is a very compact (2 L) float with active buoyancy control that can carry multiple
541 biogeochemical sensors and can be deployed in groups, collecting information on spatial
542 variability through triangulation by means of acoustic communication links as they disperse.
543 A similar idea lies behind the Wire Walker (Rainville and Pinkel, 2001; Pinkel et al., 2011)
544 which maintains a float at the surface but uses wave power to constantly yo-yo a sensor
545 package beneath it. Deploying a number of these would provide a high-frequency and
546 irregularly spaced but 3D map of biogeochemical and physical processes. These vehicles can
547 collect complete vertical profiles through 250 m of water with less than 10 minutes between
548 profiles; the time scales are shorter if the profiling depth is decreased.

549 Current satellite altimeters do not resolve the submesoscale, but do provide information
550 on the mesoscale field which can be used to diagnose where submesoscale fronts (d'Ovidio et
551 al., 2004; 2009; Lehahn et al., 2007; Deprès et al. 2011) and submesoscale vertical transport
552 (Legall et al., 2007; Isern-Fontanet et al., 2008) should occur. The Indo-German LOHAFEX
553 iron fertilization experiment (March 2009) and French KEOPS2 natural fertilization
554 experiment in the Southern Ocean (Nov 2011) used an innovative sampling strategy based on
555 this concept, with real-time identification of transport structures from the analysis of multi-
556 satellite altimetry data and surface buoy release. This approach is aimed at identifying
557 environments naturally isolated by the structure of the surface circulation, where it becomes
558 possible to study the time evolution of biophysical processes in a Lagrangian sense. More
559 generally, the use of altimetry should soon become common practice to adjust sampling
560 strategy at sea in real time (for instance, with repeated sections across submesoscale fronts, as
561 in Legall et al., 2007) according to the position of the frontal structures that can be forecast
562 with such data. In the near future, development of wide-swath altimetry by both the NASA
563 SWOT and ESA Wavemill programs would take the spatial resolution of geostrophic currents
564 to a few km, which should significantly improve our ability to identify in real time where
565 submesoscale fronts may be generated.

566 Colour satellites have long provided information on phytoplankton distributions at a
567 resolution capable of resolving the submesoscale (e.g., Gower et al., 1980), though such
568 information is often discarded by averaging the data into weekly or monthly composites.
569 Recent developments using satellites to study the biogeochemistry of the submesoscale in
570 more detail include nitrate estimates (Goes et al., 2004) and algorithms to probe community
571 composition by using the array of frequencies on multi-spectral sensors to fuller extent (e.g.,
572 Alvain et al., 2005; Uitz et al., 2009). One concern with the former is that the nitrate
573 algorithm is based on sea-surface temperature and chlorophyll measurements, so it could be

574 argued that it is not an independent measurement. It would additionally need to be
575 ascertained whether the empirical relationship underpinning it holds at the submesoscale
576 where biogeochemistry will often be far out of equilibrium. **There is also the question of**
577 **whether, to obtain an acceptable signal to noise ratio, it would be necessary to spatially**
578 **average the signal up to scales that would preclude the submesoscale from being**
579 **resolved accurately.** Nevertheless, if it proves possible to allay such concerns, the approach
580 is an appealing one as it potentially allows a much more thorough mapping of the surface
581 nitrate field than could be achieved by any ship or glider survey at a resolution which should
582 capture much of the submesoscale variability.

583 Returning to *in situ* observations, it has long been a problem that very few
584 biogeochemical properties can be accurately measured using compact autonomous sensors. It
585 is only recently that ultraviolet-based sensors capable of robust measurements of nitrate with
586 a sensitivity suitable for open ocean biogeochemistry have been developed (Pidcock et al.,
587 2010; Johnson et al., 2010). The most exciting development for submesoscale studies,
588 perhaps, is the emergence of lab-on-chip technology; the ability to use advanced engineering
589 techniques to build low energy, sophisticated but small sensors, with obvious potential for
590 deployment on any of the platforms discussed above. Of particular relevance to submesoscale
591 biogeochemistry are wave-guide-based sensors for a range of nutrients (Adornato et al.,
592 2009); miniaturized flow cytometers (e.g., Barat et al., 2010) and species-specific RNA
593 probes (e.g., Tsaloglou et al., 2011). The latter two in particular offer huge potential for
594 starting to tease apart the complexities of community composition at the submesoscale.

595

596

597

6- Conclusions

Submesoscale dynamics dominate at time and space scales that make them uniquely important to the structure and functioning of planktonic ecosystems. Resulting from interactions within the mesoscale eddy field, submesoscale flows can generate intense vertical motions at fronts, driving nutrients into the euphotic zone, and subducting organic carbon beneath it. The efficacy of submesoscale dynamics in influencing primary production and ecosystem structure depends on the local hydrography, euphotic depth, and nutrient distributions. Our lack of knowledge of the physical flows and biogeochemical responses at the submesoscale is due both to their dynamic complexity, and the practical difficulties in sampling at the appropriate time and space scales. However, recent advances in physical models, planktonic ecosystem models and ocean sampling technologies makes this an ideal time to explore the physical-chemical-biological interactions at these scales. In particular we need to gain understanding of how the intense vertical motions at the submesoscale contribute to regional-average properties such as vertical carbon and nitrogen fluxes. The strong spatial patchiness in planktonic community structure induced by submesoscale motions may lead to a significant fraction of the vertical flux being restricted to similarly small spatial and temporal scales—scales that would be missed by measurements that average over inappropriately large spatial and temporal scales. Improved understanding of the importance of submesoscale dynamics will come only through targeted interdisciplinary field and modelling programs.

Ackowledgements

All authors contributed equally to this paper. This review builds on the outcomes of a conference funded by EUR-OCEANS and Europôle Mer: *Influence of meso- and sub-mesoscale ocean dynamics on the global carbon cycle and marine ecosytems*, Centre de la Mer, Aber Wrac'h, France, June 2010. This work was supported by the joint CNRS-INSU-LEFE program & EUR-OCEANS flagship "TANGGO" (Lévy, Rivière, Martin), by the CCE-LTER program (Franks, Rivière), by NSF award 1155205 (Ferrari) and by the NERC Oceans 2025 program (Martin).

References:

Adornato, L., A. Cardenas-Valencia, E. Kaltenbacher, R.H. Byrne, K. Daly, K. Larkin, S. Hartman, M. Mowlem, R. D. Prien and V. C. Garçon (2009), In Situ Nutrient Sensors for Ocean observing systems, Proceedings of the Oceanobs'09 : Sustained Ocean observations and Information for Society Conference (Vol 2), Venice, Italy, 21-25 September 2009, Hall, J., Harrison, D.E. and Stammer D. Eds., ESA Publication WPP-306.

Alkire et al. (2012) Estimates of net community production and export using high-resolution, Lagrangian measurements of O2, NO3-, and POC through the evolution of a spring diatom bloom in the NorthAtlantic, Deep-Sea Research I, 64, 157-174.

Allen, J., Brown, L., Sanders, R., Moore, C., Mustard, A., Fielding, S., Lucas, M., Rixen, M., Savidge, G., Henson, S. (2005), Diatom carbon export enhanced by silicate upwelling in the Northeast Atlantic, Nature, 437, 728–732.

Alvain. S., Moulin C., Dandonneau Y. and Bréon F.M (2005), Remote sensing of phytoplankton groups in case 1 waters from global SeaWiFS imagery, Deep Sea Res. I, 52, 1989-2004.

Barat, D., G. Benazzi, M. Mowlem, J. M. Ruano and H. Morgan (2010), Design, simulation and characterisation of integrated optics for a microfabricated flow cytometer. Optics Communications, 283, (9), 1987-1992, doi:10.1016/j.optcom.2009.12.046.

651 Boccaletti G., R. Ferrari, and B. Fox-Kemper (2007), Mixed Layer Instabilities and
652 Restratification, J. Phys. Oceanogr., 37, 2228-2250.

653 Calil, P.H.R., and K.J. Richards (2010), Transient upwelling hot spots in the oligotrophic
654 North Pacific, J. Geophys. Res., 115, C02003, doi:10.1029/2009JC005360.

655 Capet, X., McWilliams, J., Molemaker, M., Shchepetkin, A. (2008), Mesoscale to
656 submesoscale transition in the California current system. part i: Flow structure, eddy
657 flux, and observational tests, J. Phys. Oceanogr., 38, 29–43.

658 Cavender-Bares, K. K., Rinaldo, A. and Chisholm, S. W. (2001), Microbial size spectra
659 from natural and nutrient enriched ecosystems. Limnol. Oceanogr. 46, 778–789.

660 **Chelton, D. B., R. A. Deszoeke and M. G. Schlax (1998), Geographical Variability of the**
661 **First Baroclinic Rossby Radius of Deformation, J. Phys. Oceanogr., 28, 433-460**

662 Chelton, D. B., P. Gaube, M. G. Schlax, J.J. Early and R. M. Samelson (2011), The Influence
663 of Nonlinear Mesoscale Eddies on Near-Surface Oceanic Chlorophyll, Science 334,
664 328, 10.1126/science.1208897.

665 Chisholm, S. W. (1992) Phytoplankton size. In Falkowski, P. G. and Woodhead, A. D. (eds),
666 Primary Productivity and Biogeochemical Cycles in the Sea. Plenum Press, pp. 213–
667 237.

668 Ciotti, A. M., Lewis, M. R. and Cullen, J. J. (2002) Assessment of the relationships between
669 dominant cell size in natural phytoplankton communities and the spectral shape of the
670 absorption coefficient. Limnol. Oceanogr., 47, 404–417.

671 Cipollini, P. et al. (2001), Rossby waves detected in global ocean colour data, Geophys. Res.
672 Lett., 28, 323–326, doi:10.1029/1999GL011231.

673 Cotté C., d'Ovidio F., Chaigneau A., Lévy M., Taupier-Letage I., Maté B., Guinet C. (2011),
674 Scale-dependent interactions of Mediterranean whales with marine dynamics.
675 Limnology and Oceanography, 56, (1), 219-232.

676 D'Asaro E, C. Lee, L. Rainville, R. Harcourt, L. Thomas (2011), Enhanced turbulence and
677 energy dissipation at ocean fronts, Science, 332(6027), 318-22.

678 Deprès, A., G. Reverdin and F. D'Ovidio (2011), Mechanisms and spatial variability of meso
679 scale frontogenesis in the northwestern subpolar gyre, Ocean Modelling, 39, 97-113.

680 Falkowski, P., D. Ziemann, Z. Kolber and P. K. Bienfang (1991), Role of eddy pumping in
681 enhancing primary production in the ocean, Nature, 352, 55-58.

682 **Fennel, K., Cetinic, I., D'Asaro, E., Lee, C., Perry (2011), M.J., Autonomous data**
683 **describe North Atlantic spring bloom, EOS Transactions AGU, Vol. 92, No. 50,**
684 **465-466, doi:10.1029/2011EO500002.**

685 Ferrari, R., J. C. McWilliams, V. Canuto, and D. Dubovikov (2008), Parameterization of
686 eddy fluxes at the ocean boundaries, J. Climate, 31, 2770-2789.

687 Ferrari, R. (2011), A frontal challenge for climate models, Science, 332, 316-317.

688 Fielding, S. et al. (2001), Mesoscale subduction at the Almeria-Oran front. Part 2: biophysical
689 interactions, J. Marine Systems, 30, (3-4), 287-304, doi:10.1016/S0924-
690 7963(01)00063-X.

691 Flierl, G. R., and Davis, C. S. (1993), Biological effects of Gulf stream meandering, J.
692 Marine Res., 51, 529–560.

693 Fox-Kemper, B., R. Ferrari, and R. Hallberg, 2008. Parameterization of mixed layer eddies. I:
694 Theory and diagnosis, J. Phys. Oceanogr., 38, 1145-1165.

695 Franks, P.J.S. and L.J. Walstad (1997), Phytoplankton patches at fronts: a model of formation
696 and response to transient wind events, J. Marine Res., 55, 1-30.

697 Fuchs, H.L. and Franks, P.J.S. (2010), Plankton community properties determined by
698 nutrients and size-selective feeding. Mar. Ecol. Prog. Ser., 413, 1-15.

699 Goes, J.I., H. Do, R. Gomes, T. Saino, C.S. Wong and C.W. (2004), Exploiting MODIS data
700 for estimating sea surface nitrate, Eos, 85, 449 & 454.

701 Gower, J., Denman, K., Holyer, R., (1980), Phytoplankton patchiness indicates the
702 fluctuation spectrum of mesoscale oceanic structure, Nature, 288, 157.

703 Gruber, N. et al. (2011), Eddy-induced reduction of biological production in eastern boundary
704 upwelling systems, Nature Geoscience, 4,787–792, doi:10.1038/ngeo1273

705 Guidi, L., Stemmann, L., Legendre, L., Picheral, M., Prieur, L. and Gorsky, G. (2007),
706 Vertical distribution of aggregates (>100 mm) and mesoscale activity in the
707 northeastern Atlantic: Effects on the deep vertical export of surface carbon. Limnol.
708 Oceanogr., 52, 7-18.

709 Holloway, G. and Denman, K. L. (1989), Influence of internal waves on primary production,
710 Journal of Plankton Research, 11, 409-413.

711 Hoskins, B. J., and F. P. Bretherton (1972), Atmospheric frontogenesis models: Mathematical
712 formulation and solution, J. Atmos. Sci., 29, 11–37.

713 **Hoskins, B. J. (1982), The mathematical theory of frontogenesis, Ann. Rev. Fluid Mech.,**
714 **14, 131-151.**

715 Irigoien, X., Huisman, J. and Harris, R. P. (2004) Global biodiversity patterns of marine
716 phytoplankton and zooplankton. Nature 429, 863-867.

717 Isern-Fontanet, J., G. Lapeyre, P. Klein, B. Chapron and M. W. Hect (2008), Three-
718 dimensional reconstruction of oceanic mesoscale currents from surface information, J.
719 Geophys. Res., 113, doi:10.1029/2007JC004692.

720 Johnson, K. S. S. C. Riser and D. M. Karl (2010), Nitrate supply from deep to near-surface
721 waters of the North Pacific subtropical gyre, Nature, 465, 1062-1965.

722 Joyce, T. M., L. N. Thomas and F. Bahr (2009), Wintertime observations of SubTropical
723 Mode Water formation within the Gulf Stream, Geophys. Res. Lett., 36, L02607,
724 doi:10.1029/2008GL035918.

725 Karleskind, P., M. Lévy, and L. Mémery (2011a), Modifications of mode water properties by
726 sub-mesoscales in a bio-physical model of the Northeast Atlantic, Ocean Modelling,
727 39, 47–60.

728 Karleskind, P., M. Lévy and L. Memery (2011b), Subduction of carbon, nitrogen, and oxygen
729 in the Northeast Atlantic, Journal of Geophysical Research, 116, C02025.

730 Kadko, D., L. Washburn and B. H. Jones (1991), Evidence of subduction within cold
731 filaments of the N. California Coastal Transition Zone, J. Geophys. Res., 96, 14909-
732 14926.

733 Klein, P., Hua, B., Lapeyre, G., Capet, X., Gentil, S.L. and Sasaki, H.S. (2008), Upper ocean
734 turbulence from high 3-d resolution simulations, Journal of Physical Oceanography 38,
735 1748–1763.

736 Klein, P. and Lapeyre, G. (2009), The oceanic vertical pump induced by mesoscale and
737 submesoscale turbulence, Annual Review of Marine Science, 1, 351– 375.

738 Landry, M.R. (2002), Integrating classical and microbial food web concepts: evolving views
739 from the open-ocean tropical Pacific. Hydrobiologia, 480, 29-39.

740 Landry, M.R., Ondrusek, M.E., Tanner, S.J., Brown, S.L., Constantinou, J., Bidigare, R.R.,
741 Coale, K.H. and Fitzwater, S. (2000), Biological response to iron fertilization in the
742 eastern equatorial Pacific (IronEx II). I. Microplankton community abundances and
743 biomass. Mar. Ecol. Prog. Ser., 201, 27-42.

744 Lapeyre, G., Klein, P., Hua, L., (2006a), Oceanic restratification by surface frontogenesis. J.
745 Phys. Oceanogr., 36, 1577–1590.

746 Lapeyre, G. and Klein, P. (2006b), Impact of the small scale elongated filaments on the
747 oceanic vertical pump, Journal of Marine Research, 64, 835-851.

748 **Lapeyre, G. and Klein, P. (2009), The oceanic vertical pump induced by mesoscale**
749 **eddies, Ann. Rev. Marine Science, 1,** 351-375.

750 Lathuilière, C., M. Lévy and V. Echevin (2011), Impact of eddy-driven vertical fluxes on
751 phytoplankton abundance in the euphotic layer, J. Plankton Res. 33, 5, 827-831, doi:
752 10.1093/plankt/fbq131.

753 Lathuilière, C., V. Echevin, M. Lévy and G. Madec (2010) On the role of mesoscale
754 circulation on an idealized coastal upwelling ecosystem. J. Geophys. Res., 115,
755 C09018, doi:10.1029/2009JC005827.

756 Ledwell, J. R., A. J. Watson, and C. S. Law (1998), Mixing of a tracer in the pycnocline, J.
757 Geophys. Res., 103 (C10), pp. 21,499-21,529.

758 Legall, C. P. Klein and A.-M. Tréguier (2007), Diagnosis of the Vertical Motions in a
759 Mesoscale Stirring Region, J. Phys. Ocean., 37, 1413-1423.

760 Lehahn, Y., F. d'Ovidio, M. Lévy and E. Heitzel (2007), Stirring of the Northeast Atlantic
761 spring bloom: a lagrangian analysis based on multi-satellite data, J. Geophys. Res., 112,
762 C08005, doi:10.1029/2006JC003927.

763 Lehahn, Y., F. d'Ovidio, M. Lévy, Y. Amitai and E. Heifetz (2011), Long range transport of a
764 quasi isolated chlorophyll patch by an Aghulas ring, Geophys. Res Let., 38, L16610,
765 doi:10.1029/2011GL048588.

766 Lévy, M., L. Mémery and G. Madec (1998), The onset of a bloom after deep winter
767 convection in the North Western Mediterranean Sea: mesoscale process study with a
768 primitive equation model, J. Mar. Syst., 16, 7-21.

769 Lévy, M., M. Visbeck and N. Naik (1999), Sensitivity of primary production to different
770 eddy parameterizations : a case study of the spring bloom development in the North
771 Western Mediterranean Sea, J. Mar. Res., 57, 427-448.

772 Lévy, M., L. Mémery, and G. Madec (2000), Combined effects of mesoscale processes and
773 atmospheric high-frequency variability on the spring bloom in the MEDOC area, Deep-
774 Sea Res, 47, 27-53, doi:10.1016/S0967-0637(99)00051-5.

775 Lévy, M., P. Klein and A.-M. Tréguier (2001), Impact of sub-mesoscale physics on
776 production and subduction of phytoplankton in an oligotrophic regime, Journal of
777 Marine Research, 59, 535-565.

778 Lévy, M. (2003), Mesoscale variability of phytoplankton and of new production: Impact of
779 the large scale nutrient distribution, J. Geophys. Res., 108, C11, 3358
780 10.1029/2002JC001577.

781 Lévy, M., M. Gavart, L. Mémery, G. Caniaux, and A. Paci (2005), A 4D-mesoscale map of
782 the spring bloom in the northeast Atlantic (POMME experiment): results of a
783 prognostic model, J. Geophys. Res., 110, C7, C07S21, doi: 10.1029/2004JC002588.

784 Lévy, M. P. Klein and M. Ben Jelloul (2009), New production stimulated by high-frequency
785 winds in a turbulent mesoscale eddy field, Geophysical Research Letters, 36, L16603.

786 Lévy, M. P. Klein, A.-M. Tréguier, D. Iovino, G. Madec, S. Masson and K. Takahashi (2010)
787 Modifications of gyre circulation by sub-mesoscale physics. Ocean Modelling,
788 doi:10.1016/j.ocemod.2010.04.001, 34, 1-15.

789 Lévy, M., D. Iovino, L. Resplandy, P. Klein, A.-M. Tréguier, G. Madec, S. Masson and K.
790 Takahashi (2012), Large-scale impacts of submesoscale dynamics on phytoplankton :
791 local and remote effects, Ocean Modelling. doi:10.1016/j.ocemod.2011.12.003, 43-44,
792 77-93.

793 Lewis, M. R., et al. (1986), Vertical nitrate fluxes in the oligotrophic ocean, Science, 234,
794 870-873.

795 Li, W. K. W. (2002) Macroecological patterns of phytoplankton in the northwestern North
796 Atlantic Ocean. Nature 419, 154–157.

797 Mahadevan, A. and D. Archer (2000), Modelling the Impact of Fronts and Mesoscale
798 Circulation on the Nutrient Supply and Biogeochemistry of the Upper Ocean, Journal
799 of Geophysical Research, 105, 1209-1225.

800 Mahadevan, A, Lévy, M. and L. Mémery (2004), Mesoscale variability of sea surface
801 PCO2: What does it respond to? Glob. Biogeoch. Cyc., 18, 1, GB1017
802 10.1029/2003GB002102.

803 Mahadevan, A. and A. Tandon (2006), An analysis of mechanisms for submesoscale vertical
804 motion at ocean fronts, Ocean Modelling, 14 (3-4), 241–256.

805 Mahadevan, A., A. Tagliabue, L. Bopp, A. Lenton, L. Mémery and M. Lévy (2011), Impact
806 of episodic vertical fluxes on sea surface pCO2, Phil. Trans. R. Soc. A, 369, 2009-
807 2025, doi: 10.1098/rsta.2010.0340.

808 McGillicuddy, D. J., Robinson, A.R., Siegel, D.A., Jannasch, H.W., Johnson, R., Dickey,
809 T.D., McNeil, J., Michaels, A.F., and A.H. Knap (1998), Influence of mesoscale eddies
810 on new production in the Sargasso Sea, Nature, 394, 263-266.

811 McGillicuddy, D. J., Anderson, L.A., Doney, S.C. and M.E. Maltrud (2003), Eddy-driven
812 sources and sinks of nutrients in the upper ocean: results from a 0.1 degree resolution
813 model of the North Atlantic, Global Biogeochemical Cycles, 17, doi:
814 10.1029/2002GB001987.

815 McGillicuddy, D. J. et al. (2007), Eddy/Wind Interactions Stimulate Extraordinary Mid-
816 Ocean Plankton Blooms, Science, 316, 1021-1026.

817 Martin, A.P. and Richards, K.J. (2001), Mechanisms for vertical nutrient transport within a
818 North Atlantic mesoscale eddy, Deep-Sea Research II, 48, (4-5), 757-773,
819 doi:10.1016/S0967-0645(00)00096-5.

820 Martin, A.P., Richards, K.J. and Fasham, M.J.R. (2001), Phytoplankton production and
821 community structure in an unstable frontal region, Journal of Marine Systems, 28, (1-
822 2), 65-89, doi: 10.1016/S0924-7963(00)00084-1.

823 Martin, A.P., Richards, K.J., Bracco, A. and Provenzale, A. (2002), Patchy productivity in the
824 open ocean, Global Biogeochemical Cycles, 16, 10251033,
825 doi:10.1029/2001GB001449.

826 Martin, A.P. and Pondaven, P. (2003), On estimates for the vertical nitrate flux due to eddy
827 pumping, Journal of Geophysical Research, 108, (C11), 03359,
828 doi:10.1029/2003JC001841.

829 Martin, A.P. (2003), Phytoplankton patchiness: the role of lateral stirring and mixing,
830 Progress in Oceanography, 57, (2), 125-174, doi:10.1016/S0079-6611(03)00085-5.

McWilliams, J.C. (2010), A perspective on submesoscale geophysical turbulence. In: IUTAM Symposium on Turbulence in the Atmosphere and Oceans, D. Dritschedl, ed., Springer, 131-141.

Molemaker, M.J. and J.C. McWilliams and X. Capet (2010), Balanced and Unbalanced Routes to Dissipation in an Equilibrated Eady Flow, J. Fluid Mech. 654, 35–63.

Moloney, C. L. and Field, J. G. (1991), The size-based dynamics of plankton food webs. I. A simulation model of carbon and nitrogen flows. J. Plankton Res., 13, 1003–1038.

Niewiadomska, K. Claustre, H., Prieur, L. and D'Ortenzio, F. (2008), Submesoscale physical-biogeochemical coupling across the Ligurian Current (northwestern Mediterranean) using a bio-optical glider, Limnol. Oceanogr., 53, 2210-2225. doi:10.1029/2000JC000275.

Nagai, T., A. Tandon, N. Gruber and J. McWilliams (2008), Biological and physical impacts of ageostrophic frontal circulations driven by confluent flow and vertical mixing. Dynamics of Atmospheres and Oceans 45, 229– 251.

Oschlies, A. (2002), Can eddies make ocean deserts bloom? Global Biogeochemical Cycles, 16, 1106, doi: 10.1029/2001GB001830.

Oschlies, A. and V. Garcon (1998), Eddy-induced enhancement of primary production in a model of the North Atlantic Ocean, Nature, 394, 266-269.

d'Ovidio, F., C. López, E. Hernández-García, V. Fernández (2004), Mixing structures in the Mediterranean sea from Finite-Size Lyapunov Exponents, Geophys. Res. Lett., 31, L17203.

d'Ovidio, F., J. Isern-Fontanet, C. Lopez, E. Hernandez-García and E. Garcia-Ladona (2009), Comparison between eulerian diagnostics and finite-size lyapunov exponents computed from altimetry in the Algerian basin, Deep Sea Research Part I, 56, 15–31.

d'Ovidio, F., S. De Monte, S. Alvain, Y. Dandonneau and M. Lévy (2010), Fluid dynamical niches of phytoplankton types, PNAS, doi/10.1073/pnas.1004620107

Pasquero, C., A. Bracco and A. Provenzale (2005), Impact of the spatio-temporal variability of the nutrient flux on primary productivity in the ocean, J. Geophys. Res., 110, C07005, doi:10.129/2004JC002738.

Perruche, C., P. Rivière, P. Pondaven and X. Carton (2010), Phytoplankton competition and coexistence: intrinsic ecosystem dynamics and impact of vertical mixing, J. Mar. Syst., 81, 99–111.

Perruche C., P.Rivière, G. Lapeyre, X. Carton and P. Pondaven (2011). Effects of SQG turbulence on Phytoplankton competition and coexistence. Journal of Marine Research, 69, 105-135

Pidcock, R., Srokosz, M., Allen, J., Hartman, M., Painter, S., Mowlem, M., Hydes, D. and A. Martin, (2010), A Novel Integration of an Ultraviolet Nitrate Sensor On Board a Towed

868 Vehicle for Mapping Open-Ocean Submesoscale Nitrate Variability, Journal of
869 Atmospheric and Oceanic Technology, 27, (8), 1410-1416,
870 doi:10.1175/2010JTECHO780.1.

871 Pidcock, R. (2011) Thesis (Ph.D.) - University of Southampton, School of Ocean and Earth
872 Science, pp242.

873 Pinkel, R., Goldin, M. A., Smith, J. A., Sun, O. M., Aja, A. A., Bui, M. N. and Hughen, T.
874 (2011), The Wirewalker: A Vertically Profiling Instrument Carrier Powered by Ocean
875 Waves. J. Atmos. Ocean. Tech., 28, 426–435, doi:10.1175/2010JTECHO805.1

876 Poulin, F.J. and Franks, P.J.S. (2010), Size-structured planktonic ecosystems: constraints,
877 controls and assembly instructions. J. Plankton Res., 32, 1121-1130.

878 Rainville, L., and Pinkel, R. (2001), Wirewalker: An autonomous wave-powered vertical
879 profiler. Jour. Atmos. Ocean. Tech., 18, 1048–1051.

880 Rassoulzadegan, F. and Sheldon, R.W. (1986), Predator-prey interactions of
881 nanozooplankton and bacteria in an oligotrophic marine environment. Limnol.
882 Oceanogr., 31, 1010-1021.

883 Resplandy, L., M. Lévy, F. d'Ovidio and L. Merlivat (2009), Impact of submesoscale
884 variability in estimating the air-sea CO2 exchange: Results from a model study of the
885 POMME experiment, Glob. Biogeo. Cyc., 23, GB1017, doi:10.1029/2008GB003239.

886 Rossi V., C. Lopez, J. Sudre, E. Hernandez-Garcıa and V. Garçon (2008). Comparative study
887 of mixing and biological activity of the Benguela and Canary upwelling systems.
888 Geophys. Res. Lett., 3, L11602.

889 Ruiz, J., D. Macias, et al. (2004). Turbulence increases the average settling velocity of
890 phytoplankton cells. Proceedings of the National Academy of Sciences of the United
891 States of America, 101, 17720-17724.

892 Santoleri, R., V. Banzon, S. Marullo, E. Napolitano, F. D'Ortenzio and R. Evans (2003).
893 Year-to-year variability of the phytoplankton bloom in southern Adriatic Sea (1998-
894 2000): SeaWiFS observations and modelling study. J. Geophys. Res., 108, C9, 8122,
895 DOI:10.1029/2002JC001636.

896 Spall, M.A. (1995), Frontogenesis, subduction, and cross-front exchange at upper ocean
897 fronts. J. Geophys. Res. 100, 2543–2557.

898 Taylor, J., and R. Ferrari (2010), Buoyancy and wind-driven convection at a mixed-layer
899 density fronts, J. Phys. Oceanogr., 40, 1222-1242.

900 Taylor, J., and R. Ferrari (2011a), The role of density fronts in the onset of phytoplankton
901 blooms, Geophys. Res. Lett., 38, L23601, doi:10.1029/2011GL049312.

902 Taylor, J., and R. Ferrari (2011b), A shutdown of turbulent convection can trigger the spring
903 phytoplankton bloom, L & O, 56, 2293-2307.

Tew Kai, E., Rossi, V., Sudre, J., Weimerskirch, H., Lopez, C., Hernandez-Garcia, E., Marsac, F. and Garçon, V. (2009), Top marine predators track Lagrangian coherent structures PNAS, doi:10.1073/pnas.0811034106.

Thomas (2005), Destruction of potential vorticity by winds, J. Phys. Ocean., 35, 2457-2466.

Thomas, L. and Ferrari, R. (2008), Friction, frontogenesis, and the stratification of the surface mixed layer, J. Phys. Oceanogr., 38, 2501–2518.

Thomas L. N. and T.M. Joyce (2010), Subduction on the Northern and Southern Flanks of the Gulf Stream, J. Phys. Oceanogr, 40, 429-438, doi:10.1175/2009JPO4187.1.

Townsend, D. W., L. M. Cammen, P. M. Holligan, D. E. Campbell and N. R. Pettigrew (1994), Causes and consequences of variability in the timing of spring phytoplankton blooms, Deep Sea Res. Part I, 41, 747.

Tsaloglou, M.-N., M. M. Bahi, E. M. Waugh, H. Morgan and M. Mowlem (2011), On-chip real-time nucleic acid sequence-based amplification for RNA detection and amplification. Analytical Methods, 3, 2127-2133, doi:10.1039/C1AY05164D.

Uitz J., H. Claustre, B. Gentili, D. Stramski (2010), Phytoplankton class-specific primary production in the world's oceans: Seasonal and interannual variability from satellite observations, Global Biogeochemical Cycles, 24, GB3016, 1-19, doi:10.1029/2009GB003680.

Uz, B. et al. (2001), Pumping of nutrients to ocean surface waters by the action of propagating planetary waves, Nature, 409, 597–600, doi:10.1038/35054527.

Williams, R.G. and M.J. Follows (2003), Physical transport of nutrients and the maintenance of biological production, In `Ocean Biogeochemistry: The role of the ocean carbon cycle in global change', Edited by M. Fasham, Springer, ISBN: 3-540-42398-2, pp 19-51.

Yentsch, C. S. and Phinney, D. A. (1989) A bridge between ocean optics and microbial ecology. Limnol. Oceanogr. 34, 1694–1705.

930 **Figures**

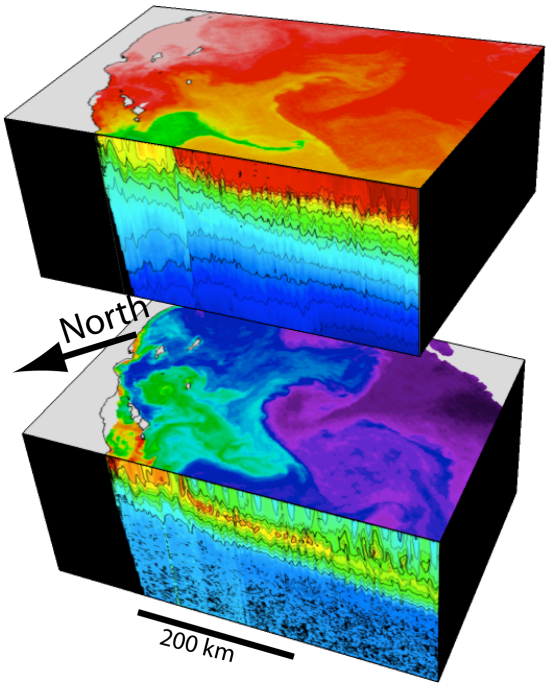

931

932 **Figure 1.** Three-dimensional views looking southeastward from Point Conception
933 (California, USA) showing MODIS satellite remote sensing data combined with *in situ* glider
934 data (www.sccoos.org/data/spray/). Top: temperature. Bottom: chlorophyll *a*. Ocean
935 temperature is a good proxy for density in this part of the ocean. **The surface mesoscale**
936 **patterns seen in the temperature and chlorophyll *a* can also be seen as subsurface**
937 **fluctuations in the isopycnal surfaces. The strong fronts and eddies are sites of strong**
938 **submesoscale dynamics which can drive local responses of the phytoplankton.**

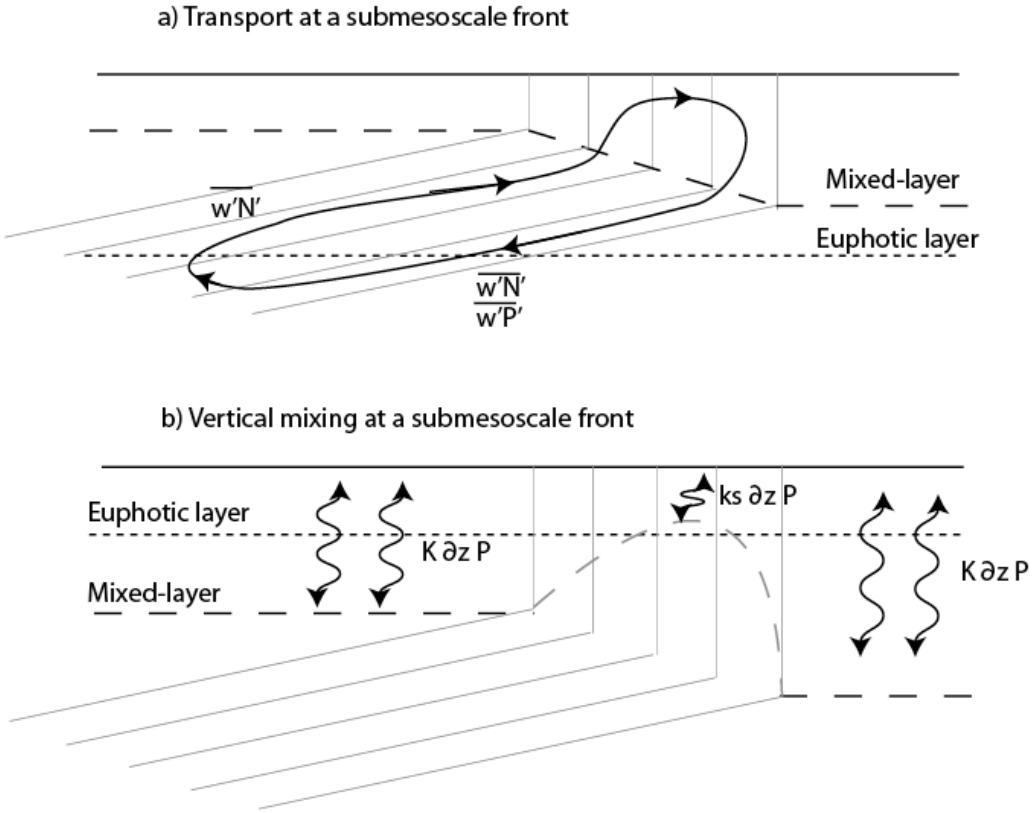

939

940 **Figure 2.** Schematic representation of how submesoscale advection and diffusion impacts
941 biogeochemestry. a) Advection: the upwelling branch of the ageostrophic circulation at a
942 submesoscale front provides nutrient to the euphotic layer while the downwelling branch
943 exports excess nutrient and organic material below the euphotic layer, along isopycnals.
944 These processes prevail in situations where primary production is controlled by the
945 availability of nutrients; in such cases the mixed-layer is shallower than the euphotic depth.
946 b) Vertical mixing: the reduction of vertical diffusivity at a mesoscale front is illustrated here
947 as a reduction in the the mixed-layer depth and in vertical mixing coefficient (K > ks) ; this
948 process prevails when primary production is inhibited by strong vertical diffusivity, which
949 causes phytoplankton to be mixed in and out of the euphotic layer; at the front, this mixing is
950 reduced and phytoplankters remain in the well lit euphotic zone, which favors their growth
951 with respect to out of front areas.

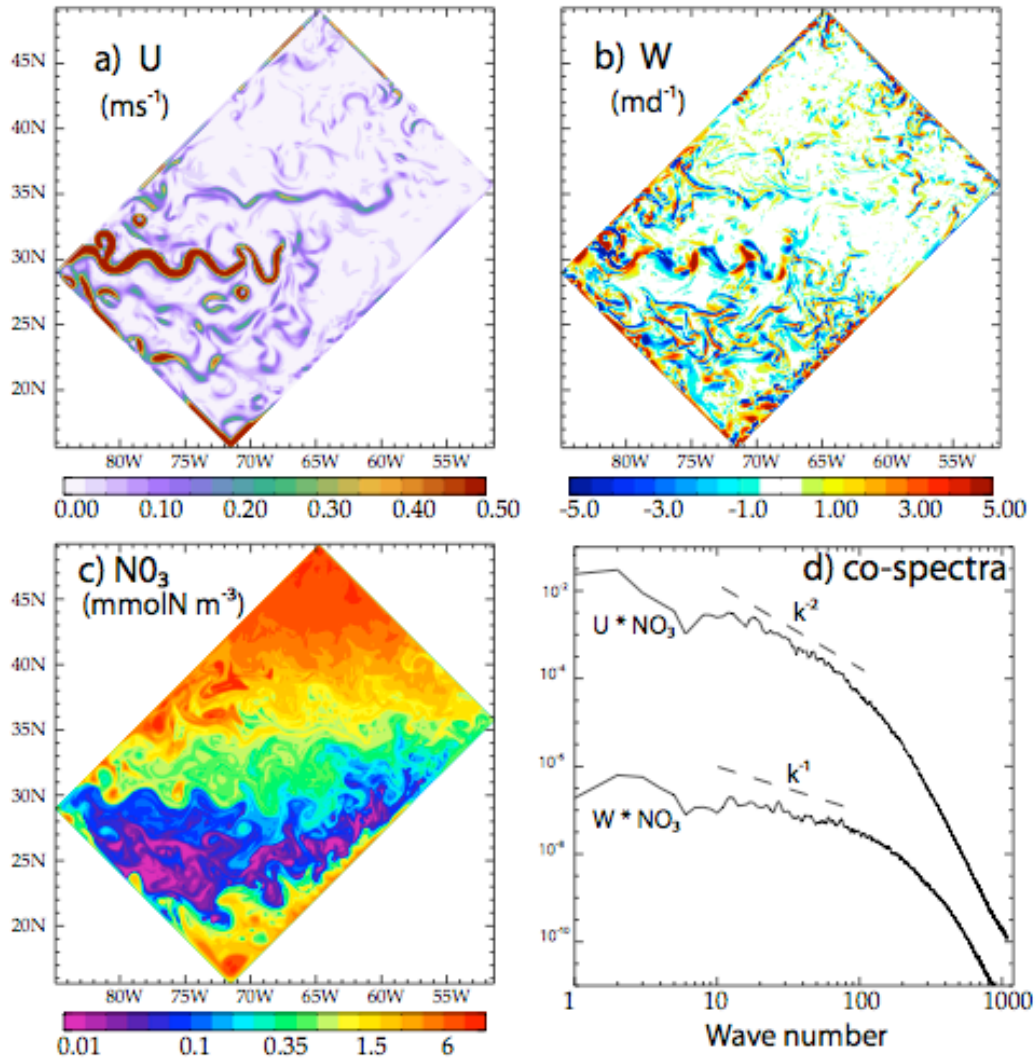

952

953 **Figure 3. Snapshots of a) modulus of horizontal velocity (U), b) vertical velocity (W)**
954 **and c) Nitrate concentration (NO_3, in log scale) from an idealized submesoscale-**
955 **resolving model simulation representative of the Northwest Atlantic or Northwest**
956 **Pacific subtropical to subpolar regions. Model fields are shown at 50 m depth, in winter**
957 **(Dec 1st). d) Co-spectra of U * NO_3 and W* NO_3, plotted in log-log scale.**

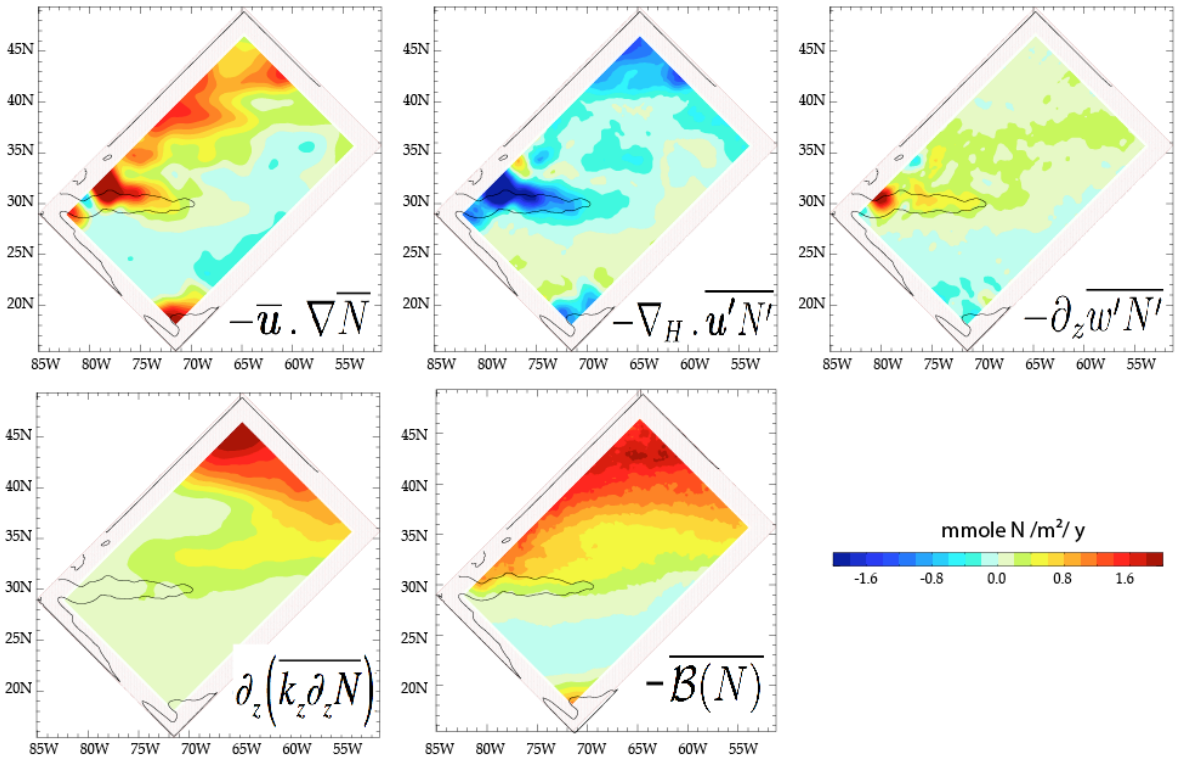

958

959 **Figure 4**. Contribution of all terms in the nitrate (N= NO_3) equation (Eq. 1) from an
960 idealized model simulation representative of the Northwest Atlantic or Northwest Pacific
961 subtropical to subpolar regions. The terms are averaged over the year and over the euphotic
962 depth, as in Eq. 2 The model is at equilibrium, hence the biological term
963 $\int_{1year}\int_{z=0}^{Zeupho}\overline{B(N)}dzdt$ is exactly balanced by the sum of the four physical terms
964 $\int_{1year}\int_{z=0}^{Zeupho}[-\overline{u}.\nabla\overline{N}-\nabla_H\cdot\overline{u'N'}-\partial_z\overline{w'N'}+\partial_z\left(\overline{k_z\partial_z N}\right)]dzdt$. The black contour shows the annual
965 mean location of the model's idealized Gulf Stream or Kuroshio current. The mean of the
966 fields, denoted with an overbar, is defined in this computation as a coarse-grained running
967 average of 2° width.

968

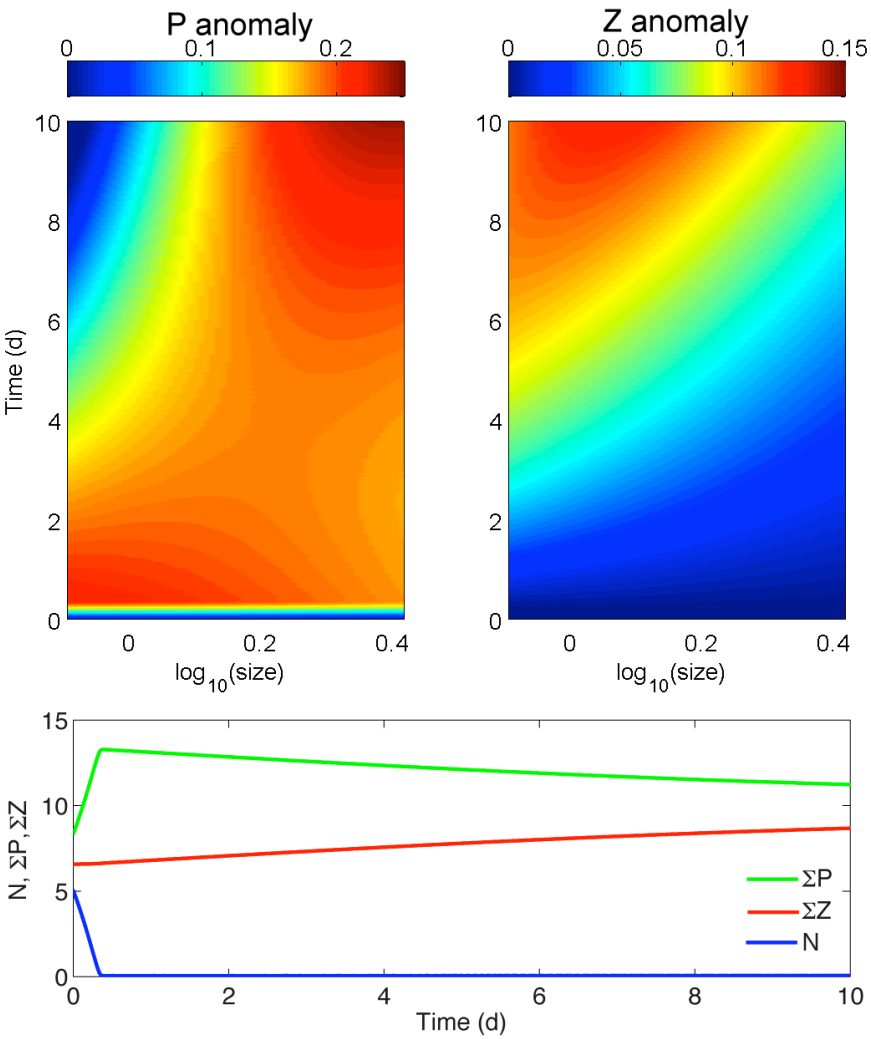

Figure 5. Response of size-structured ecosystem to a nutrient pulse at time 0. Top left panel: phytoplankton biomass anomalies (log10 of the ratio of the time-dependent distribution to the initial distribution). **Top right panel: zooplankton biomass anomalies. Bottom panel: Time series of nutrients, total phytoplankton, and total zooplankton. Model is a time-dependent version of PF10. In the first 4 days after the nutrient pulse the smallest phytoplankton bloom, followed by an increase of their grazers. The grazer control of the smallest phytoplankton allows the larger phytoplankton to bloom. This bloom slowly propagates to the largest phytoplankton. Each bloom is followed by an increase in population of that size class's grazers. Note the rapid uptake of the nutrient pulse.**

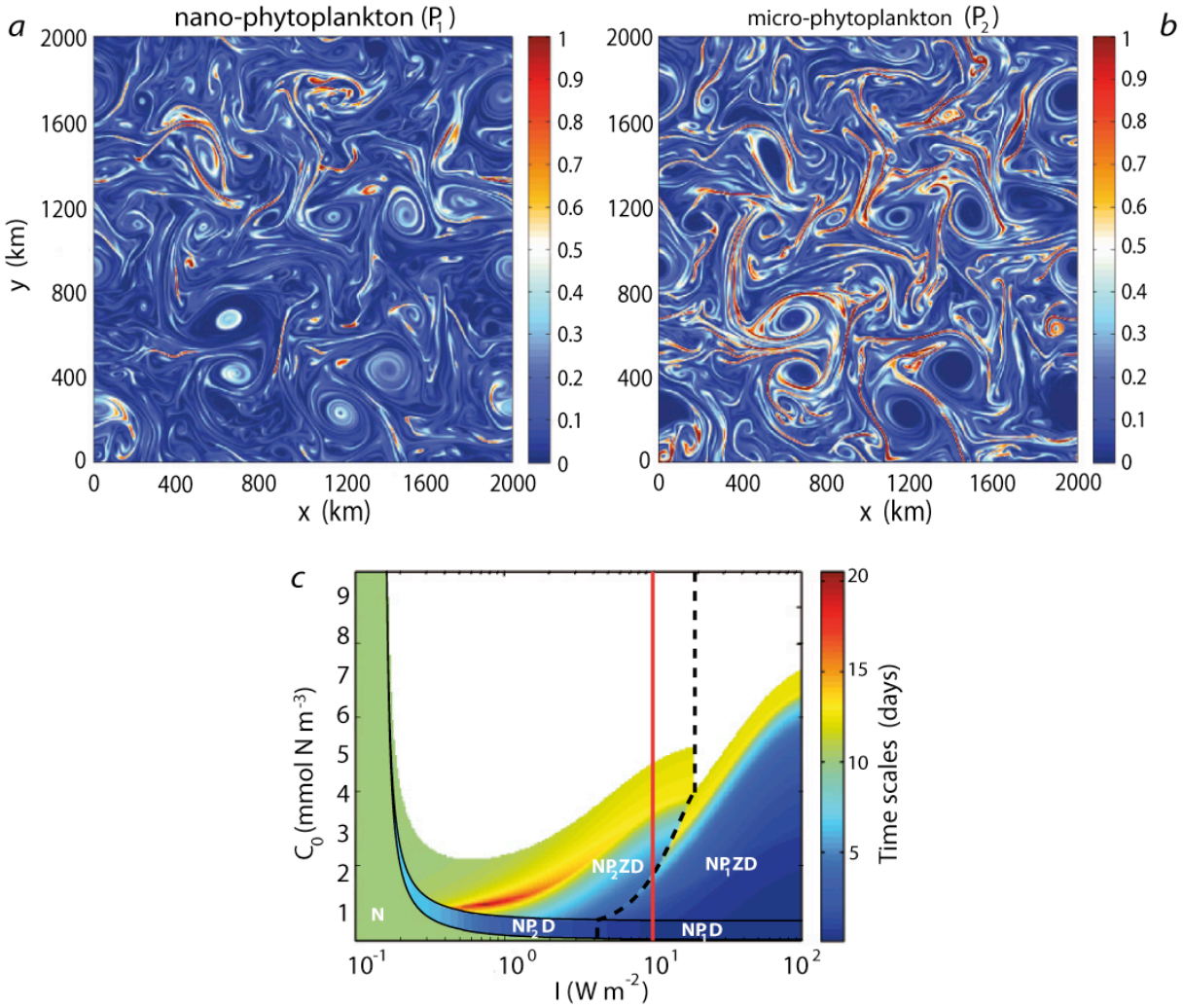

980

981 **Figure 6.** Upper panels: spatial distribution snapshot of two phytoplankton size classes
982 (a: P_1 and b: P_2) in a submesoscale-resolving model (colour bar in mmol N m^{-3}) . Panel c:
983 equilibrium community structure under different total nitrogen (C_0) and irradiance (I)
984 conditions (note that irradiance axis is logarithmic). White letters indicate the state variables
985 that exist at equilibrium for the given irradiance and nutrient concentration. Note that P_1 and
986 P_2 do not coexist at equilibrium. Time scale to reach equilibrium (in days) is indicated in
987 colours (white area corresponds to limit cycles at equilibrium). Dashed line separates the two
988 regions in which either P_1 or P_2 exists at equilibrium. Red line indicates the position in the
989 parameter space corresponding to the SQG simulation with a fixed irradiance level of 10
990 Wm^{-2} (adapted from Perruche et al., 2010, 2011). The coexistence of P1 and P2 in the SQG
991 model is due to the perturbations of the ecosystem by mesoscale and submesoscale motions,
992 maintaining the ecosystem out of equilibrium.